PHILOSOPHICAL TRANSACTIONS A

rsta.royalsocietypublishing.org

Research

Article submitted to journal

Subject Areas:
Aeronomy, Giant Planets, Neptune

Keywords:
Aeronomy, Ionosphere, H_3^+

Author for correspondence:
L. Moore
e-mail: moore@bu.edu

Atmospheric implications of the lack of H_3^+ detection at Neptune

L. Moore[1], J.I. Moses[2], H. Melin[3], T.S. Stallard[3], and J. O'Donoghue[4]

[1]Boston University, USA.
[2]Space Science Institute, USA.
[3]University of Leicester, UK.
[4]JAXA Institute of Space and Astronautical Science, Japan.

H_3^+ has been detected at all of the solar system giant planets aside from Neptune. Current observational upper limits imply that there is far less H_3^+ emission at Neptune than rudimentary modeling would suggest. Here, we explore via modeling a range of atmospheric conditions in order to find some that could be consistent with observational constraints. In particular, we consider that the upper atmosphere might be much cooler than it was during the 1989 Voyager 2 encounter, and we examine the impact of an enhanced influx of external material that could act to reduce H_3^+ density. Resulting ionosphere models that are consistent with existing H_3^+ observational constraints have an exospheric temperature of 450 K or less, 300 K lower than the Voyager 2 value. Alternatively, if a topside CO influx of $2x10^8$ cm^{-2} s^{-1} is imposed, the upper atmospheric temperature can be higher, up to 550 K. The potential cooling of Neptune's atmosphere is relevant for poorly understood giant planet thermospheric energetics, and would also impact aerobreaking maneuvers for any future spacecraft. Such a large CO influx, if present, could imply Triton is a very active moon with prominent atmospheric escape, and/or that Neptune's rings significantly modify its upper atmosphere, and the introduction of so much exogenic material would complicate interpretation of the origin of species observed in Neptune's lower atmosphere.

THE ROYAL SOCIETY PUBLISHING

1. Introduction

The H_3^+ ion is rapidly formed primarily by collisions between H_2 and H_2^+ and is therefore expected to be important in a variety of astronomical environments [1,2]. Since its first remote detection in Jupiter's auroral ionosphere [3], it has served as a remarkably useful probe of upper-atmospheric densities, temperatures and velocities at Jupiter (e.g., [4–6]), Saturn (e.g., [7,8]), and Uranus [9], but it has remained undetected thus far at Neptune [10]. Such remote measurements serve as effective constraints in an otherwise difficult-to-sample atmospheric region. They also provide key insights into coupling processes from above and below, as the simplicity of the chemistry in gas giant ionospheres, which consist mainly of H_3^+ and H^+ above the homopause, is temporarily disrupted by any exogenic material [11].

Observations of quantities relevant to H_3^+ in Neptune's upper atmosphere are limited by its distance and small angular size. Voyager 2, during its 1989 fly-by, used solar occultation measurements to derive an exospheric temperature of 750±150 K [12], and found stratospheric temperatures of ~170 K [13,14]. Interpolated temperature at the expected H_3^+ altitudes is roughly 550 K. Recent ground-based observations have used this average temperature to place an upper limit on H_3^+ column density, based on a non-detection of bright H_3^+ lines near 4 μm, of $1.0^{+1.2}_{-0.16}\times10^{13}$ m^{-2} [10] (see also [15,16]). These vibration–rotation transitions of the ν_2 fundamental band [17] have been used to derive non-auroral H_3^+ column densities at Jupiter, Saturn, and Uranus, typically of order 10^{15} m^{-2} [18], 10^{16} m^{-2} [8], and 10^{15} m^{-2} [9], respectively.

Consistent with the limited observational constraints, there are few published models of Neptune's upper atmosphere. Lyons [19] modeled the sharp layers of electron density revealed by radio occultation experiments in Neptune's lower ionosphere [20]. While that model truncates at 1500 km altitude (above the 1 bar pressure level), the modeled H_3^+ column density can be conservatively estimated as $>5\times10^{13}$ m^{-2}, i.e., more than a factor of 5 larger than the current upper limit. A recent model, again focused on Neptune's lower ionosphere, finds an H_3^+ column density that is roughly comparable or even larger [21]. Therefore, while modeling studies of Neptune's ionosphere are limited, with objectives other than upper atmospheric H_3^+, there appears to be a significant discrepancy between the amount of H_3^+ expected and historical observational upper limits.

Here, we conduct a range of model simulations in order to find combinations of conditions in Neptune's upper atmosphere that could be consistent with the present lack of H_3^+ detection. As H_3^+ emission is driven exponentially by temperature, we first examine the possibility that Neptune's atmosphere is cooler than found by Voyager 2 in 1989. Next, as H_3^+ reacts readily with other molecules, we also investigate how its density might be reduced by enhanced influxes of external material, such as CO or dust particles from Triton/other satellites/Neptune's rings, or material from elsewhere in the local system. The models used and modeling approaches followed are described in §2. Results are introduced and discussed in §3, with implications for Neptune's atmosphere outlined in §4.

2. Methods

(a) Model description

The majority of H_3^+ ions in giant planet ionospheres are in photochemical equilibrium (PCE), as the H_3^+ chemical lifetime is much shorter than the transport timescale at most altitudes, and therefore the ion continuity equation simplifies to equating local production and loss (i.e., $P_s = L_s$) [22,23]. While transport processes are still relevant – and highly so for H^+, especially at high altitude – the dominance of chemical loss at low altitudes justifies the use of one-dimensional (1-D) simulations for those regions, which offer the advantages of simplicity and computational freedom over more dynamically comprehensive 3-D simulations.

Two models are adopted in the present work. The simulations are conducted in 1-D, owing to the prevalence of PCE for H_3^+ distributions, and there are separate neutral and plasma modules in order to enable a more computationally-efficient exploration of ion chemistry.

The neutral module is described in detail by *Moses and Poppe* [24], and is actually a combination of a meteoroid ablation code [25,26] with the Caltech/JPL 1-D KINETICS photochemical model [27,28]. KINETICS solves the coupled mass-continuity equations as a function of pressure, and includes molecular and eddy diffusion transport terms. It has proved to be effective and highly adaptable, having been applied to all of the giant planets, and currently treats 70 hydrocarbon and oxygen species that interact via ~500 recently-updated chemical reactions [24,29]. Input for the meteoroid ablation code follows from revised constraints on interplanetary dust fluxes in the outer Solar System based on in situ spacecraft data [30]. The resulting oxygenated and hydrocarbon mixing ratios are in agreement with a wide range of observational constraints [24]. Therefore, after adjusting the KINETICS simulations for the solar and geometric conditions explored here, the resulting neutral atmospheres serve as an excellent background for exploring realistic ion-neutral photochemistry at Neptune.

Plasma densities and temperatures follow from another 1-D model called BU1DIM, which has recently been generalized for application to any planetary atmosphere, and includes significantly expanded chemistry (see [31] and references therein). BU1DIM describes the time- and altitude-dependent structure of an ionosphere by solving the coupled continuity, momentum and energy equations for all ion species of interest. The primary effect of magnetic fields on 1-D ionospheric calculations is to constrain the plasma motion (e.g., introducing a $\sin^2 I$ term into the expression for vertical ion drift velocity, where I is the magnetic dip angle [32,33]). Therefore – partly due to incomplete knowledge of Neptune's magnetic field, and partly due to the predominance of PCE at H_3^+ altitudes – magnetic field lines are considered to be vertical here. Modelled ion production rates follow from the attenuation of solar Extreme UltraViolet (EUV; 10-124 nm) and soft X-ray photons (combined, the XUV) [34], which are extrapolated to Neptune based on measurements from the Thermosphere Ionosphere Mesosphere Energetics and Dynamics Solar EUV Experiment (TIMED/SEE) [35]. Aside from solar XUV radiation, no other sources of ionization are considered in this work.

Early theoretical models of giant planet ionospheres predicted electron densities that were up to an order of magnitude too large based on later spacecraft measurements, with Saturn exhibiting the most extreme discrepancy [36,37]. One commonly adopted mechanism for reducing modelled electron densities in order to better match observations was to convert H^+ into a short-lived molecular ion via the reaction

$$H^+ + H_2(\nu \geq 4) \rightarrow H_2^+ + H \tag{2.1}$$

Without the introduction of some form of ion-neutral charge-exchange reaction, such as (2.1), modelled H^+ – and hence electron density, n_e – is unrealistically large, as the radiative recombination rate coefficient for H^+ is extremely slow (~10^{-12} cm^3 s^{-1} for typical giant planet thermospheric electron temperatures) [38]. The (2.1) reaction rate is thought to be near its maximum kinetic value [39,40], however the fraction of molecular hydrogen in the 4^{th} or higher vibrational state is not constrained by observations at present. As two of the dominant sources of vibrationally excited H_2 have been shown to be photon-induced fluorescence and dissociative recombination of H_3^+ ions – two solar-driven processes – we scale fractional H_2 vibrational populations calculated for Jupiter [41] by $\frac{1}{r^2}$ to account for the diminution of solar photons with distance. Thus adjusted, the *Majeed et al.* [41] $H_2(\nu \geq 4)$ results are then interpolated onto the appropriate Neptune pressure grid. Further model inputs and specific settings are discussed in relation to their corresponding results in §2(b).

(b) Variations in the background atmosphere

Planetary H_3^+ emission is optically thin [18] and depends on the temperature and density of the plasma. Therefore, the lack of H_3^+ detection at Neptune is most likely caused by some combination

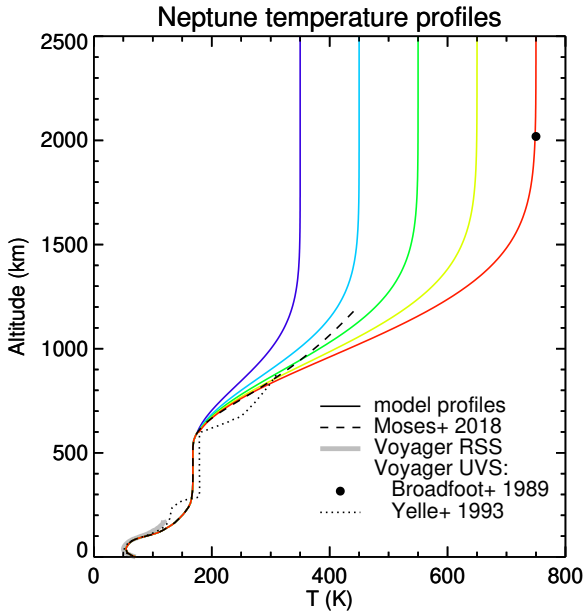

Figure 1. Colored solid lines represent variations in thermal structure explored in this study. The red is the reference atmosphere based on infrared observations [42], combined in Moses et al. [44], and Voyager 2 constraints from its 1989 fly-by [12,13], with various aspects of the Voyager data indicated by the gray shaded and dotted lines, and the filled circle.

of two factors: (a) Neptune's upper atmosphere is cooler than found by Voyager 2 in 1989, and/or (b) there is some unknown mechanism reducing the amount of H_3^+ in Neptune's ionosphere. This section outlines the parameter variations that we explore in order to find model atmospheres that are consistent with the present H_3^+ upper limit.

Constraints on thermal structure in Neptune's atmosphere are based on analysis of Voyager 2 fly-by data and on a variety of infrared observations. Solar occultation measurements by Voyager's Ultraviolet Spectrometer (UVS) found the topside, or exospheric (T_{exo}), temperature to be 750±150 K [12] (filled circle in Figure 1). Radio occultations by Voyager's Radio Science Subsystem (RSS), sensitive to the upper troposphere and lower stratosphere, found a local minimum of ~50 K [20] (gray shaded region in Figure 1). Subsequent detailed analysis of the UVS observations were also used to constrain temperatures in the upper stratosphere [13] (dotted line in Figure 1). Finally, remote infrared observations [42,43] led to a temperature profile in Neptune's troposphere and stratosphere that was mostly consistent with Voyager data (approximately represented by the dashed line in Figure 1, taken from [44]).

The thermal structure used in the reference model is given by the red curve in Figure 1. Other colored curves represent additional possible atmospheres that are still consistent with observations in the troposphere and stratosphere, differing only in exospheric temperature and the resulting upper atmospheric temperature gradient. There is sufficient justification for considering exospheric temperatures different from what Voyager observed in 1989. First, the Voyager measurement sampled one location on Neptune, so it is reasonable to assume that temperature will vary spatially. Second, we know that temperatures in giant planet upper atmospheres – and, of course, planetary atmospheres in general – are temporally variable. There is recent evidence at Saturn [45,46] and Uranus [9] for significant temperature variations as well as long term cooling. Finally, we don't yet fully understand the energetics of giant planet upper atmospheres: observed exospheric temperatures at all four giant planets are hundreds of Kelvin hotter than predictions based on solar heating alone [47]. Upper atmospheric energy budgets are likely further modified by internal forcing, such as due to gravity waves, which have been shown to be present at Jupiter [48] and Saturn [49], though the degree of resulting heat deposition is unclear at present [50].

Thermal structure primarily affects overall atmospheric extent. It also strongly affects H_3^+ emission, as it is driven exponentially by temperature [51]. Also relevant for the lack of H_3^+ detection at Neptune is H_3^+ column density, which is marginally reduced in a cooler atmosphere,

owing to a smaller column depth. H_3^+ is also highly reactive, however, and so can be removed by contaminants introduced into the pristine H^+ and H_3^+ upper ionosphere. At Saturn, we now have ample evidence for an inflow of ring material modifying ionospheric chemistry [8,11,52,53]. All of the giant planets are also exposed to interplanetary dust particles (IDPs), primarily from various families of comets. Dust grains can also originate from active plumes on satellites such as Io, Enceladus, and Triton. Constraints on these influxes are limited, typically based on model comparisons with observations sensitive to atmospheric constituents at stratospheric pressure levels. In other words, such model-data comparisons are insensitive to possible upper-atmospheric concentrations, and those concentrations are responsible for modifying H_3^+ densities. Further ionospheric modifications might derive from internal forcing, such as due to gravity waves breaking in the lower thermosphere, though the effect on H_3^+ is minimal due to its relatively short chemical lifetime [54].

The upper-atmospheric "contaminant" explored here is CO. While the reference atmosphere contains both internal and external sources of CO [44], only external sources lead to sufficient thermospheric abundances to affect the ionosphere. It acts to remove H_3^+ via charge-exchange reactions, just as a range of other possible contaminants would. Given the lack of upper-atmospheric observational constraints, we choose to focus on CO for simplicity, but emphasize that some combination of contaminants could similarly affect the ionosphere. In addition, there is an enormous CO abundance in Neptune's stratosphere, which must have an external source based on the increase of the observed mixing ratio from the troposphere to stratosphere (e.g., [55]). Current literature tends to favor a cometary impact within the last couple hundred years as that source (e.g., [21,24] and references therein), however models which consider a topside influx of $\leq 2\times10^8$ CO molecules cm^{-2} s^{-1} are also consistent with stratospheric constraints on CO and lead to much larger thermospheric CO concentrations than the cometary scenario [24].

Figure 2a presents the reference Neptune atmosphere used in this study, representative of conditions at 45°S planetocentric latitude. Its vertical structure follows from the red temperature profile in Figure 1, and its oxygenated species are generated by two sources: a flux of IDPs based on recent dust dynamical modeling [30], and a large cometary impact approximately 200 years ago (as described in [24]). Figure 2b then illustrates the full range of variations in CO evaluated. First, solid lines correspond to the above scenario, colored according to the assumed T_{exo}. Second, dotted lines consider that Neptune's CO is due solely to IDPs, also colored by T_{exo}. Note that solid and dotted lines only differ below 600 km altitude (i.e., they overlap above 600 km), demonstrating that higher altitude CO comes from IDPs in the reference model. Finally, a range of different topside influxes of CO are represented by various types of dashed lines, as indicated in the legend. The five different thermal scenarios illustrated in Figure 1 are all evaluated for the maximum CO influx of 2×10^8 cm^{-2} s^{-1}, color coded according to T_{exo}. For reduced CO influxes, spanning 10^5 - 10^8 cm^{-2} s^{-1} only the T_{exo} = 750 K atmosphere is considered.

Finally, it should be noted that modifying the effective rate of reaction (2.1) is likely not a primary solution to the lack of H_3^+ at Neptune. A larger electron density, such as would follow from a reduced (2.1) rate, would lead to smaller H_3^+ densities via an increase in their dissociative recombination reaction with electrons, but electron densities are constrained to be $<10^3$ cm^{-3} above ~1700 km altitude by Voyager 2 radio occultation measurements [20].

3. Results and discussion

We now present ionospheric results based on the neutral atmospheres shown in Figure 2. In 3(a), we show altitude variations in H_3^+ number density. In 3(b), we column-integrate the model parameters in order to compare directly with observational constraints. Finally, in 3(c), we discuss the choice of CO as the representative "external material" within the model and speculate on the possibility and source of such large influxes.

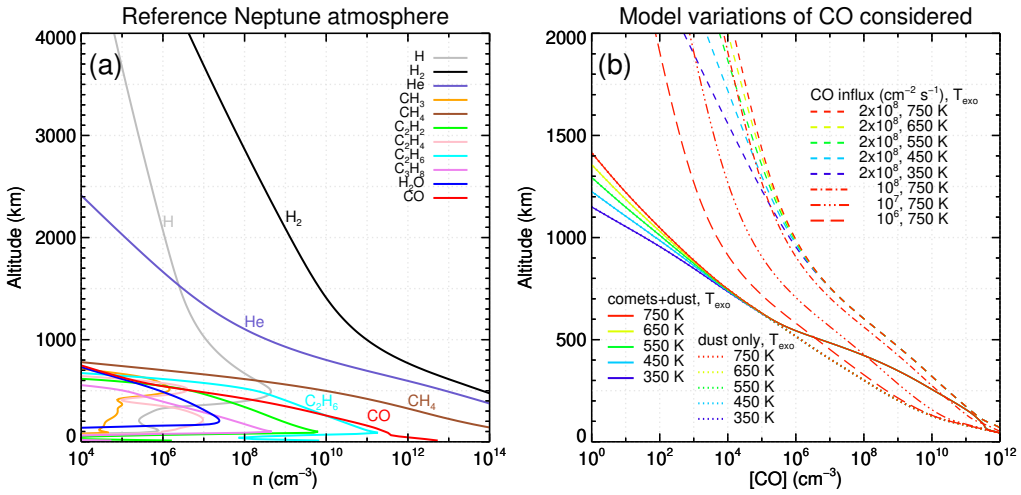

Figure 2. (a) Reference Neptune atmosphere at 45°S planetocentric latitude with T_{exo}=750 K and CO based on cometary and dust sources (see [24]), plotted in altitude to highlight the upper atmosphere. (b) Variations in CO considered in this work due to T_{exo} (line colors) and CO source (line types). CO from the "dust only" and "comet+dust" model types are identical above 600 km altitude (i.e., the dotted and solid curves overlap there). Similarly, topside CO influxes of <10^6 cm^{-2} s^{-1} (not shown) are indistinguishable from the "dust only" model below ~1000 km. Note that the axes are scaled differently in each panel.

(a) Variability in H_3^+ density

The reference Neptune ionosphere model, based on Figure 2a, is shown in Figure 3a. It represents local noon densities at 45°S planetocentric latitude. This latitude was chosen as a reasonable compromise between the geometry of Voyager observations and recent observational constraints [10]. The Voyager 2 RSS egress was at ~45°S planetographic latitude (gray shading in Figure 1), and the UVS exit was at 49°S (filled circle in Figure 1). Recent ground-based H_3^+ observations searched for emission integrated over Neptune's dayside between 17-20 August 2017. Neptune's sub-solar latitude over this time period was 25°S, but the diurnally-averaged solar irradiance is quite similar at 45°S. This has been demonstrated for other giant planets (e.g., [31]), as modelled H_3^+ column densities are comparable over a wide range of latitudes in the summer hemisphere.

Figure 3b illustrates the effect of the neutral background variations from Figure 2b on modelled H_3^+ densities. The solid lines represent changes due to variations in atmospheric temperature, colored according to T_{exo}. Cooler atmospheres exhibit a decreased altitudinal extent of H_3^+, consistent with the relative atmospheric collapse, but peak H_3^+ number densities are actually marginally increased due to the reduced attenuation of solar photons at higher altitudes. CO in Neptune's atmosphere for these profiles is assumed to come from interplanetary dust (IDPs) and a cometary impact 200 years ago [24]. Dotted lines, which overlap with solid lines, investigate the possibility that Neptune's CO is instead solely due to IDPs. As shown in Figure 2b, the "comet+dust" and "dust only" CO scenarios differ only below ~600 km altitude, and therefore it is unsurprising that their effect on H_3^+ densities, which are significant only above ~700 km altitude, is indistinguishable. Dashed lines then examine a scenario in which an influx of 2×10^8 CO molecules cm^{-2} s^{-1} is introduced at the top of the atmosphere. Modelled H_3^+ densities are significantly lower than either of the two previous scenarios, as H_3^+ is rapidly converted to HCO^+, though the qualitative behavior with T_{exo} variations is similar. Finally, the remaining line types indicated in the legend examine slightly reduced topside CO influxes for the T_{exo} = 750 K case. From the perspective of H_3^+ density, any CO influx <10^6 cm^{-2} s^{-1} is effectively indistinguishable from the alternative scenarios currently used to explain stratospheric observational constraints.

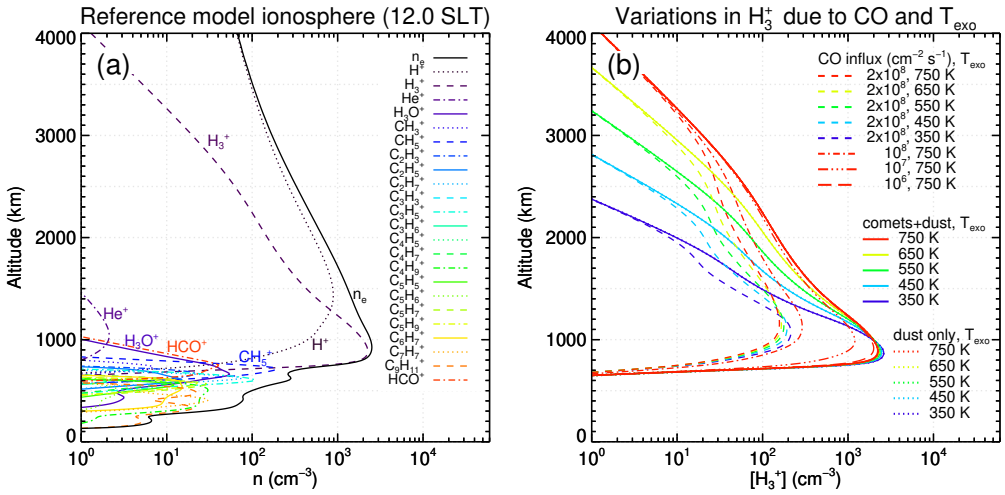

Figure 3. (a) Reference Neptune ionospheric model at noon solar local time (SLT). Ion species are indicated in the legend. (b) Variations in modelled H_3^+ at 12 SLT resulting from different T_{exo} values (line colors) and CO sources (line types). Note that, as CO from the "dust only" and "comet+dust" model types are identical above 600 km altitude (Figure 2b), H_3^+ values are also identical over that region, and thus solid and dotted lines overlap completely in this panel.

(b) Comparison to observational constraints

The most recent observational constraints on H_3^+ at Neptune come from ground-based spectroscopic observations near 4 μm [10]. In that campaign, Melin et al. [10] aligned the spectral slit along the planetographic equator and integrated for 15.4 h over 4 nights. The 1.5 arcsec wide slit covered nearly the entire southern hemisphere of the planet, and stretched up to ~15°N latitude. In order to search for a faint H_3^+ emission, the data were summed spatially: i.e., integrated across Neptune's entire dayside over this region. The upper limit on spectral intensity above the continuum at the location of bright H_3^+ spectral lines was found to be 12^{+15}_{-10} nW m^{-2} sr^{-1} μm^{-1}. Combined with an estimated temperature of 550 K near the H_3^+ peak, this led to an upper limit on H_3^+ column density of $1.0^{+1.2}_{-0.16} \times 10^{13}$ m^{-2}, a 30% improvement over previous constraints [15,16].

In order to best compare with observations, which are column integrated, we must derive similar modelled parameters. However, as H_3^+ emission is tightly coupled to the vertical temperature and gradients present in the atmosphere, and as imperfect knowledge of those gradients can induce ambiguity in the derived column-integrated densities and temperatures [31], it is best to compare with the more fundamental upper limit on H_3^+ emission rather than the derived column density. Therefore, Figure 4 presents model results for both H_3^+ column densities (4a) and total emission (4b). These are mean daytime values, meaning they are the average from 6-18 Solar Local Time (SLT), consistent with the observations. Column densities follow directly from Figure 3b. Total H_3^+ emission is calculated by combining the line list of Neale et al. [56] with the partition function and total emission formulation of Miller et al. [57]. This treatment depends on the vertical structure of both H_3^+ density and temperature. H_3^+ has been found to be in quasi-LTE with the surrounding neutral atmosphere at the other giant planets, at least at altitudes within ~5 scale heights of the density peak (e.g., [58,59]). Therefore, we take the H_3^+ temperature to be the neutral temperature (Figure 1) for these calculations.

Based on Figure 4a, H_3^+ column density is most strongly affected by enhanced CO influxes. An atmosphere with T_{exo} of 350 K has a column density that is 30% lower than one with T_{exo} of 750 K, whereas the impact of a CO influx of 2×10^8 cm^{-2} s^{-1} leads to a reduction by more than a factor of 10. This relative importance of CO influx is minimized for cooler atmospheres, however.

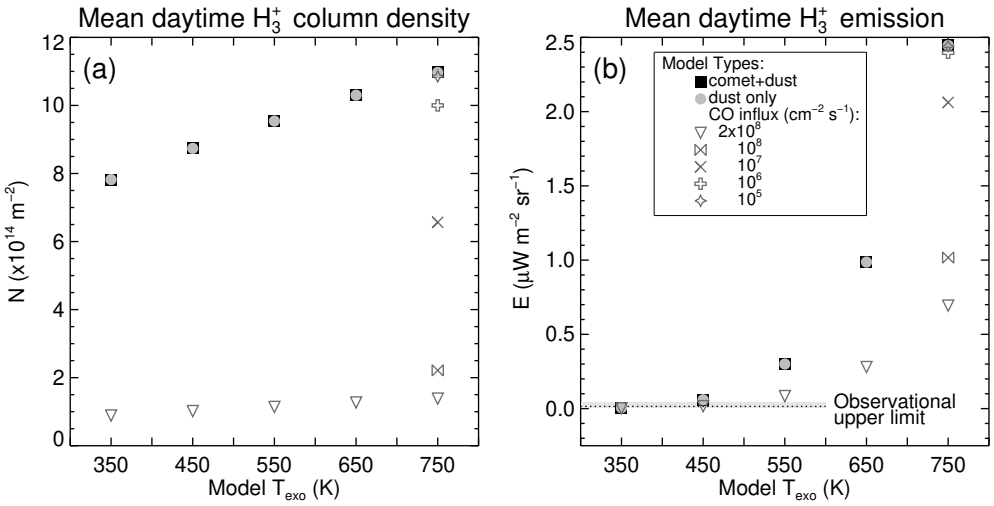

Figure 4. (a) Mean daytime (=6-18 SLT here) H_3^+ column density for each model simulation. (b) Mean daytime (6-18 SLT) H_3^+ emission for each model simulation. Symbols and colors in the legend represent modelled variations in CO (shown in Figure 2), while T_{exo} variations are indicated along the abscissa. The gray shaded region, split by a dotted line, indicates the upper limit, including error bars, on H_3^+ emission from ground-based observations [10].

In Figure 4b, showing total H_3^+ emission, the situation is reversed and temperature becomes the more important parameter. If Neptune's atmosphere is still as warm as it was during the Voyager 2 fly-by (T_{exo} = 750 K), then H_3^+ emission could vary by more than a factor of 3, depending on the thermospheric CO concentration. However, H_3^+ emission drops off precipitously with cooler and cooler atmospheres, to the point that CO influx has no noticeable impact on the already weak emission when T_{exo} is $\leq$450 K.

The gray shaded region and dotted line in Figure 4b represent the observational limits from Melin et al. [10], recast in terms of total H_3^+ emission. The model atmospheres with T_{exo} of 350 K and 450 K are consistent with the observations, regardless of the thermospheric CO content. When we consider that there remain a number of model input paramaters that we have not varied here, it is possible that the T_{exo}=550 K atmosphere is also consistent with these constraints, provided there is a topside CO influx of 2×10^8 cm^{-2} s^{-1}. It is clear, however, that no reasonable combination of model parameters is consistent with the present non-detection of H_3^+ at Neptune when the atmosphere is warm. Modelled H_3^+ total emission for both the T_{exo} 650 K and 750 K cases far exceeds the observational upper limit of $15^{+42}_{-3.3}$ nW m^{-2} sr^{-1}, regardless of CO input.

(c) Discussion of external influx

Based on Figure 4b, there is at least one scenario where the maximum-allowed CO influx of 2×10^8 cm^{-2} s^{-1} could help explain the lack of H_3^+ detection: when T_{exo} is also 550 K. None of the other reduced CO influxes considered can sufficiently remove H_3^+ in the thermosphere. If this large CO influx is real, where does it come from?

Triton, as an active moon, is one possible source, though current estimates for atmospheric escape from Triton are much smaller than the CO fluxes considered here. For example, based largely on Voyager data, a range of studies find N, N_2, N^+ and hydrogen escape rates roughly of order 10^{25} s^{-1} [60–65]. Deposited globally at Neptune, this would translate to influxes of ~10^5 cm^{-2} s^{-1}. However, the CO/N_2 mixing ratio at Triton is ~6×10^{-4}, meaning CO escape rates and resulting influxes are likely even lower. Of course, these external influxes may be concentrated locally at Neptune, such as at low latitudes, like Encealadus' plumes at Saturn [66], but likely not

as drastically as would be required, and in any case such local concentration would only mean H_3^+ at other latitudes remained undiminished. That said, CO in Triton's atmosphere appears to be controlled by seasonal transport and/or atmospheric escape [67], and it may not be in steady-state [68]. Therefore, Triton remains an unlikely but intriguing possibility as the source of CO considered here.

Neptune's dusty rings present another appealing possible source of ionospheric contaminant. During the Cassini spacecraft's end-of-mission proximal orbits, mass fluxes into Saturn's atmosphere of up to 20×10^4 kg s^{-1} were derived from in situ measurements of infalling ring material [52,53,69,70], leading to significant modification of its equatorial ionosphere [11,71, 72]. Cassini Ion and Neutral Mass Spectrometer spectra in Saturn's upper atmosphere were unexpectedly rich [52], showing stable signal out to 100 mass per charge (u), with a strong 28u peak containing significant CO contribution [73]. Neptune's rings are of course less massive than Saturn's, but the implicated source at Saturn was the tenuous D68 ringlet [52]. The bulk of the ring mass flux measured by Cassini was concentrated at Saturn's equator, yet there were still substantial charged particle "ring rain" effects on mid-latitude H_3^+ concentrations [8,53]. Therefore, Neptune's rings as a source of ionospheric modification remain as a possibility.

4. Conclusions

H_3^+ has regularly been monitored at all of the giant planets except Neptune. Current observational upper limits on H_3^+ column density are at least a factor of 5 lower than straightforward ionospheric models predict, however these upper limits are also based on Voyager 2 temperature measurements from ~30 years ago. In order to address these model-data discrepancies, we performed model explorations of two primary factors that could affect H_3^+ emission: variations in upper atmospheric temperature, and variations in thermospheric CO concentration due to enhanced topside influxes.

As H_3^+ emission is driven exponentially by temperature, the simplest way to generate an ionosphere consistent with the H_3^+ upper limits is to reduce the upper atmospheric temperature. We find that if the topside temperature, T_{exo}, is $\leq$450 K, then modelled H_3^+ emission is within current constraints. For warmer atmospheres, up to T_{exo} of 550 K, H_3^+ density must be reduced significantly to avoid exceeding the H_3^+ emission upper limit. A topside CO influx of 2×10^8 cm^{-2} s^{-1} could fill this role by converting H_3^+ to HCO^+. (Larger topside CO influxes would lead to stratospheric abundances in excess of current observations [24].) In this scenario, the HCO^+ column density is modeled to be 4.3×10^{14} m^{-2}. Therefore, if H_3^+ continues to evade detection, and if there is indeed a significant CO influx present, then it might be possible to observe HCO^+ instead. Such a measurement could place a soft constraint on the topside CO influx, and thus be used to infer thermospheric temperatures when combined with H_3^+ upper limits.

The potential for Neptune's atmosphere to be significantly cooler than what Voyager 2 found is intriguing, and would also have important implications for any future spacecraft considering aerobraking as a means of orbital insertion. Further, with the James Webb Space Telescope and other advanced facilities coming online in the next decade, the possibility of utilizing H_3^+ as a probe of Neptune's upper atmosphere, as at the other giant planets, is significantly increased. The explanation behind the high observed exospheric temperatures at the giant planets is a longstanding problem, and measurements of H_3^+ at Neptune could help by expanding the available comparative planetary studies.

Data Accessibility. Only model "data" were utilized here and are available from L.M. upon request.

Authors' Contributions. L.M. conceived of and designed the study, performed the ionospheric simulations, and drafted the manuscript. J.I.M. contributed to the design of the study, and performed neutral model simulations. H.M., T.S.S. and J.O'D. performed the Neptune H_3^+ observations (H.M. as lead), and advised on H_3^+ emission calculations. All authors reviewed, edited, and approved the manuscript.

Competing Interests. We declare we have no competing interests.

Funding. L.M. and J.I.M. were supported by the National Aeronautics and Space Administration (NASA) under Grant 80NSSC19K0546 issued through the Solar System Workings Program.

Acknowledgements. We are grateful to the TIMED/SEE PI, Tom Woods, and his team for providing us with the solar flux dataset and associated routines for extrapolation to planets.

References

1. S. Miller, J. Tennyson, T. R. Geballe, and T. Stallard, "Thirty years of H3+ astronomy," *Reviews of Modern Physics*, no. May 2020, pp. 1–67, 2020.
2. T. Oka, "H3+, the ideal probe for in situ measurement of the Galactic cosmic rays," *Philosophical transactions of the Royal Society A*, vol. 377, pp. 1–9, 2019.
3. P. Drossart, J.-P. Maillard, J. Caldwell, S. Kim, J. Watson, W. Majewski, J. Tennyson, S. Miller, S. Atreya, J. Clarke, J. Waite Jr., and R. Wagener, "Detection of H3+ on Jupiter," *Nature*, vol. 340, pp. 539–541, 1989.
4. R. Johnson, H. Melin, T. Stallard, C. Tao, J. Nichols, and M. Chowdhury, "Mapping H3+ Temperatures in Jupiter's Northern Auroral Ionosphere Using VLT-CRIRES," *Journal of Geophysical Research A: Space Physics*, vol. 123, pp. 1–19, 2018.
5. T. Uno, Y. Kasaba, C. Tao, T. Sakanoi, M. Kagitani, S. Fujisawa, H. Kita, and S. V. Badman, "Vertical emissivity profiles of Jupiter's northern H3+ and H2 infrared auroras observed by Subaru/IRCS," *Journal of Geophysical Research: Space Physics*, vol. 119, pp. 10219– 10241, 2014.
6. B. M. Dinelli, A. Adriani, A. Mura, F. Altieri, A. Migliorini, and M. L. Moriconi, "JUNO/JIRAM's view of Jupiter's H3+ emissions," *Philosophical transactions of the Royal Society A*, vol. 377, 2019.
7. T. S. Stallard, K. H. Baines, H. Melin, T. J. Bradley, L. Moore, J. O'Donoghue, S. Miller, M. N. Chowdhury, S. V. Badman, H. J. Allison, and E. Roussos, "Local-time averaged maps of H3+ emission, temperature and ion winds," *Philosophical Transactions of the Royal Society A: Mathematical, Physical and Engineering Sciences*, vol. 377, no. 2154, 2019.
8. J. O'Donoghue, L. Moore, J. Connerney, H. Melin, T. S. Stallard, S. Miller, and K. H. Baines, "Observations of the chemical and thermal response of 'ring rain' on Saturn's ionosphere," *Icarus*, vol. 322, no. April 2018, pp. 251–260, 2018.
9. H. Melin, L. N. Fletcher, T. S. Stallard, S. Miller, L. M. Trafton, L. Moore, J. O. Donoghue, R. J. Vervack Jr, N. Dello Russo, L. Lamy, C. Tao, and M. N. Chowdhury, "The H3+ ionosphere of Uranus: decades-long cooling and local-time morphology," *Philosophical transactions of the Royal Society A*, vol. 377, 2019.
10. H. Melin, L. N. Fletcher, T. S. Stallard, R. E. Johnson, J. O. Donoghue, L. Moore, and P. T. Donnelly, "The quest for H3+ at Neptune: deep burn observations with NASA IRTF iSHELL," *Monthly Notices of the Royal Astronomical Society*, vol. 474, pp. 3714–3719, 2018.
11. L. Moore, T. E. Cravens, I. Mueller-Wodarg, M. E. Perry, J. J. Waite, R. Perryman, A. Nagy, D. Mitchell, A. Persoon, J.-E. Wahlund, and M. W. Morooka, "Models of Saturn's Equatorial Ionosphere Based on In Situ Data From Cassini's Grand Finale," *Geophysical Research Letters*, vol. 45, pp. 1–10, 2018.
12. A. L. Broadfoot, S. K. Atreya, J. L. Bertaux, J. E. Blamont, A. J. Dessler, T. M. Donahue, W. T. Forrester, D. T. Hall, F. Herbert, J. B. Holberg, D. M. Hunter, V. A. Krasnopolsky, S. Linick, J. I. Lunine, J. C. McConnell, H. W. Moos, B. R. Sandel, N. M. Schneider, D. E. Shemansky, G. R. Smith, D. F. Strobel, and R. V. Yelle, "Ultraviolet spectrometer observations of Neptune and Triton," *Science*, vol. 246, pp. 1459–66, dec 1989.
13. R. V. Yelle, F. Herbert, B. R. Sandel, R. J. Vervack Jr, and T. M. Wentzel, "The distribution of hydrocarbons in Neptune's upper atmosphere," *Icarus*, vol. 104, pp. 38–59, 1993.
14. J. Bishop, S. K. Atreya, P. N. Romani, B. R. Sandel, and F. Herbert, "Voyager 2 ultraviolet spectrometer solar occultations at Neptune: Constraints on the abundance of methane in the stratosphere," *Journal of Geophysical Research*, vol. 97, no. E7, p. 11681, 1992.
15. H. Feuchtgruber and T. Encrenaz, "The infrared spectrum of Neptune at 3.5-4.1 microns: Search for H3+ and evidence for recent meteorological variations," *Astronomy and Astrophysics*, vol. 403, no. 1, pp. 7–10, 2003.
16. H. Melin, T. Stallard, S. Miller, M. B. Lystrup, L. M. Trafton, T. C. Booth, and C. Rivers, "New limits on H3+ abundance on Neptune using Keck NIRSPEC," *Monthly Notices of the Royal Astronomical Society*, vol. 410, no. 1, pp. 641–644, 2011.

17. T. Oka, "Chemistry, astronomy and physics of H3+," *Philosophical transactions. Series A, Mathematical, physical, and engineering sciences*, vol. 370, pp. 4991–5000, nov 2012.
18. H. A. Lam, N. Achilleos, S. Miller, J. Tennyson, L. M. Trafton, T. R. Geballe, and G. E. Ballester, "A Baseline Spectroscopic Study of the Infrared Auroras of Jupiter," *Icarus*, vol. 393, pp. 379–393, 1997.
19. J. R. Lyons, "Metal ions in the atmosphere of Neptune," *Science*, vol. 267, no. 5198, pp. 648–651, 1995.
20. G. Lindal, "The atmosphere of Neptune: an analysis of radio occultation data acquired with Voyager 2," *The Astronomical Journal*, vol. 103, no. 3, pp. 967–982, 1992.
21. M. Dobrijevic, J. C. Loison, V. Hue, T. Cavalié, and K. M. Hickson, "1D photochemical model of the ionosphere and the stratosphere of Neptune," *Icarus*, vol. 335, no. July 2019, 2020.
22. L. Moore, M. Galand, A. J. Kliore, A. F. Nagy, and J. O 'Donoghue, "Saturn's Ionosphere," in *Saturn in the 21st Century* (K. H. Baines, F. M. Flasar, N. Krupp, and T. S. Stallard, eds.), ch. 8, p. arXiv:1701.05178, Cambridge: Cambridge University Press, 2018.
23. R. Schunk and A. Nagy, *Ionospheres: Physics, Plasma Physics, and Chemistry*. Cambridge, UK: Cambridge University Press, 2nd ed., 2009.
24. J. I. Moses and A. R. Poppe, "Dust Ablation on the Giant Planets: Consequences for Stratospheric Photochemistry," *Icarus*, vol. 297, pp. 33–58, 2017.
25. J. I. Moses, "Meteoroid ablation in Neptune's atmosphere," *Icarus*, vol. 99, pp. 368–383, oct 1992.
26. J. Moses, "Dust ablation during the Shoemaker-Levy 9 impacts," *Journal of Geophysical Research*, vol. 102, no. E9, pp. 21,619–21,643, 1997.
27. M. Allen, Y. L. Yung, and J. W. Waters, "Vertical Transport and Photochemistry in the Terrestrial Mesosphere and Lower Thermosphere (50-120 km)," *Journal of Geophysical Research*, vol. 86, no. A5, pp. 3617–3627, 1981.
28. Y. L. Yung, M. Allen, and J. P. Pinto, "Photochemistry of the atmosphere of Titan: comparison between model and observations," *The Astrophysical Journal Supplement Series*, vol. 55, pp. 465–506, 1984.
29. J. I. Moses, E. S. Armstrong, L. N. Fletcher, A. J. Friedson, P. G. J. Irwin, J. A. Sinclair, and B. E. Hesman, "Evolution of stratospheric chemistry in the Saturn storm beacon region," *Icarus*, vol. 261, pp. 149–168, 2015.
30. A. R. Poppe, "An improved model for interplanetary dust fluxes in the outer Solar System," *Icarus*, vol. 264, pp. 369–386, 2016.
31. L. Moore, H. Melin, J. O'Donoghue, T. Stallard, J. Moses, M. Galand, S. Miller, and C. Schmidt, "Modelling H3+ in planetary atmospheres: effects of vertical gradients on observed quantities," *Philosophical transactions of the Royal Society A*, vol. 377, no. 67, pp. 1–19, 2019.
32. L. Moore, M. Mendillo, I. Müller-Wodarg, and D. Murr, "Modeling of global variations and ring shadowing in Saturn's ionosphere," *Icarus*, vol. 172, pp. 503–520, dec 2004.
33. H. Rishbeth and O. K. Garriott, *Introduction to Ionospheric Physics*, vol. 14. New York: Academic Press, 1st ed., 1969.
34. M. Galand, L. Moore, B. Charnay, I. Mueller-Wodarg, and M. Mendillo, "Solar primary and secondary ionization at Saturn," *Journal of Geophysical Research*, vol. 114, p. A06313, jun 2009.
35. T. N. Woods, F. Eparvier, S. Bailey, P. Chamberlin, J. Lean, G. Rottman, S. Solomon, W. Tobiska, and D. Woodraska, "Solar EUV Experiment (SEE): Mission overview and first results," *Journal of Geophysical Research*, vol. 110, no. A1, p. A01312, 2005.
36. J. H. Waite and T. E. Cravens, "Current review of the Jupiter, Saturn, and Uranus ionospheres," *Advances in Space Research*, vol. 7, no. 12, pp. 119–134, 1987.
37. T. Majeed, J. Waite, S. Bougher, R. Yelle, G. Gladstone, J. McConnell, and a. Bhardwaj, "The ionospheres–thermospheres of the giant planets," *Advances in Space Research*, vol. 33, pp. 197–211, jan 2004.
38. Y. Kim and J. Fox, "The chemistry of hydrocarbon ions in the Jovian ionosphere," *Icarus*, vol. 112, pp. 310–324, 1994.
39. D. L. Huestis, "Hydrogen collisions in planetary atmospheres, ionospheres, and magnetospheres," *Planetary and Space Science*, vol. 56, pp. 1733–1743, nov 2008.
40. D. L. Huestis, S. W. Bougher, J. L. Fox, M. Galand, R. E. Johnson, J. I. Moses, and J. C. Pickering, "Cross Sections and Reaction Rates for Comparative Planetary Aeronomy," *Space Science Reviews*, vol. 139, pp. 63–105, jul 2008.

41. T. Majeed, J. McConnell, and R. Yelle, "Vibrationally excited H2 in the outer planets thermosphere: Fluorescence in the Lyman and Werner bands," *Planetary and Space Science*, vol. 39, no. 11, pp. 1591–1606, 1991.
42. G. S. Orton, L. N. Fletcher, I. de Pater, J. I. Moses, E. Lellouch, R. Moreno, B. M. Swinyard, M. D. Hofstadter, and T. K. Greathouse, "Thermal emission constraints on the atmospheres of Uranus and Neptune," in *Workshop on the Study of the Ice Giant Planets, LPI Contributions*, p. 2002, 2014.
43. H. Feuchtgruber, E. Lellouch, G. Orton, T. D. Graauw, B. Vandenbussche, B. Swinyard, R. Moreno, C. Jarchow, F. Billebaud, T. Cavalié, S. Sidher, and P. Hartogh, "The D/H ratio in the atmospheres of Uranus and Neptune from Herschel-PACS observations," *Astronomy & Astrophysics*, vol. 126, pp. 1–9, 2013.
44. J. I. Moses, L. N. Fletcher, T. K. Greathouse, G. S. Orton, and V. Hue, "Seasonal stratospheric photochemistry on Uranus and Neptune," *Icarus*, vol. 307, pp. 124–145, 2018.
45. T. Koskinen, B. Sandel, R. Yelle, D. Strobel, I. Müller-Wodarg, and J. Erwin, "Saturn's variable thermosphere from Cassini/UVIS occultations," *Icarus*, vol. 260, pp. 174–189, 2015.
46. Z. Brown, T. Koskinen, I. Müller-Wodarg, R. West, A. Jouchoux, and L. Esposito, "A pole-to-pole pressure–temperature map of Saturn's thermosphere from Cassini Grand Finale data," *Nature Astronomy*, 2020.
47. S. Miller, A. Aylward, and G. Millward, "Giant Planet Ionospheres and Thermospheres: The Importance of Ion-Neutral Coupling," *Space Science Reviews*, vol. 116, pp. 319–343, jan 2005.
48. K. I. Matcheva and D. F. Strobel, "Interaction of Gravity Waves with Ionospheric Plasma: Implications for Jupiter's Ionosphere," *Icarus*, vol. 152, pp. 347–365, 2001.
49. K. I. Matcheva and D. J. Barrow, "Small-scale variability in Saturn's lower ionosphere," *Icarus*, vol. 221, pp. 525–543, nov 2012.
50. R. V. Yelle and S. Miller, "Jupiter's Thermosphere and Ionosphere," in *Jupiter: The Planet, Satellites and Magnetosphere* (F. Bagenal, T. E. Dowling, and W. B. McKinnon, eds.), ch. 9, pp. 185–218, Cambridge: Cambridge University Press, 2004.
51. S. Miller, T. Stallard, J. Tennyson, and H. Melin, "Cooling by H3+ emission," *The Journal of Physical Chemistry A*, vol. 117, no. 39, pp. 9770–9777, 2013.
52. J. H. J. Waite, R. Perryman, M. Perry, K. Miller, J. Bell, T. E. Cravens, C. R. Glein, J. Grimes, M. Hedman, J. Cuzzi, T. Brockwell, B. Teolis, L. Moore, D. Mitchell, A. Persoon, W. S. Kurth, J.-E. Wahlund, M. Morooka, L. Hadid, S. Chocron, J. Walker, A. Nagy, R. Yelle, S. Ledvina, R. Johnson, W. Tseng, O. J. Tucker, and W.-H. Ip, "Chemical Interactions between Saturn's Atmosphere and Rings," *Science*, vol. 362, no. eaat2382, pp. 1–12, 2018.
53. H.-w. Hsu, J. Schmidt, S. Kempf, F. Postberg, G. Moragas-klostermeyer, M. Seiß, H. Hoffmann, M. Burton, S. Y. Ye, W. S. Kurth, M. Horányi, N. Khawaja, F. Spahn, D. Schirdewahn, J. O'Donoghue, L. Moore, J. Cuzzi, G. H. Jones, and R. Srama, "Cosmic Dust Analyzer onboard Cassini Collects Material from Saturn's Main Rings," *Science*, vol. accepted, pp. 1–28, 2018.
54. D. J. Barrow and K. I. Matcheva, "Modeling the effect of atmospheric gravity waves on Saturn's ionosphere," *Icarus*, vol. 224, pp. 32–42, may 2013.
55. E. Lellouch, R. Moreno, and G. Paubert, "A dual origin for Neptune's carbon monoxide?," *Astronomy & Astrophysics*, vol. 430, pp. L37–L40, 2005.
56. L. Neale, S. Miller, and J. Tennyson, "Spectroscopic Properties of the H3+ Molecule: A New Calculated Line List," *The Astrophysical Journal*, vol. 464, pp. 516–520, 1996.
57. S. Miller, T. Stallard, H. Melin, and J. Tennyson, "H3+ cooling in planetary atmospheres," *Faraday Discussions*, vol. 147, p. 283, 2010.
58. L. Moore, M. Galand, I. Müller-Wodarg, R. Yelle, and M. Mendillo, "Plasma temperatures in Saturn's ionosphere," *Journal of Geophysical Research*, vol. 113, p. A10306, oct 2008.
59. C. Tao, S. V. Badman, and M. Fujimoto, "UV and IR auroral emission model for the outer planets: Jupiter and Saturn comparison," *Icarus*, vol. 213, pp. 581–592, jun 2011.
60. Y. L. Yung and J. R. Lyons, "Triton: Topside ionosphere and nitrogen escape," *Geophysical Research Letters*, vol. 17, no. 10, pp. 1717–1720, 1990.
61. D. F. Strobel and M. E. Summers, "The photochemistry of methane in the atmosphere of Triton," *Geophysical Research Letters*, vol. 17, no. 10, pp. 1729–1732, 1990.
62. B. R. Sandel, F. Herbert, A. J. Dessler, and T. W. Hill, "Aurora and airglow on the night side of Neptune," *Geophysical Research Letters*, vol. 17, no. 10, pp. 1693–1696, 1990.
63. M. E. Summers and D. F. Strobel, "Triton's atmosphere: A source of N and H for Neptune's magnetosphere," *Geophysical Research Letters*, vol. 18, no. 12, pp. 2309–2312, 1991.

64. V. A. Krasnopolsky, B. R. Sandel, F. Herbert, and R. J. Vervack Jr, "Temperature, N2, and N density profiles of Triton's atmosphere: Observations and model," *Geophysical Research Letters*, vol. 98, no. E2, pp. 3065–3078, 1993.
65. H. Lammer, "Mass loss of N2 molecules from Triton by magnetospheric plasma interaction," *Planetary and Space Science*, vol. 43, no. 7, pp. 845–850, 1995.
66. B. L. Fleshman, P. A. Delamere, F. Bagenal, and T. Cassidy, "The roles of charge exchange and dissociation in spreading Saturn's neutral clouds," *Journal of Geophysical Research*, vol. 117, p. E05007, may 2012.
67. E. Lellouch, C. D. Bergh, B. Sicardy, S. Ferron, and H.-U. Käufl, "Detection of CO in Triton's atmosphere and the nature of surface-atmosphere interactions," *Astronomy & Astrophysics*, vol. 512, no. L8, pp. 2–7, 2010.
68. J. L. Elliot, D. F. Strobel, X. Zhu, J. A. Stansberry, L. H. Wasserman, and O. G. Franz, "The Thermal Structure of Triton's Middle Atmosphere," *Icarus*, vol. 143, pp. 425–428, 2000.
69. M. E. Perry, J. H. W. Jr, D. G. Mitchell, K. E. Miller, and T. E. Cravens, "Material Flux From the Rings of Saturn Into Its Atmosphere," *Geophysical Research Letters*, vol. 45, pp. 1–8, 2018.
70. D. Mitchell, M. Perry, D. Hamilton, J. Westlake, P. Kollmann, H. Smith, J. Carbary, J. J. Waite, R. Perryman, H.-W. Hsu, J.-E. Wahlund, M. Morooka, L. Hadid, A. Persoon, and W. Kurth, "D-Ring Dust Falling into Saturn's Equatorial Upper Atmosphere," *Science*, vol. accepted, pp. 1–18, 2018.
71. T. E. Cravens, L. Moore, J. H. J. Waite, R. Perryman, M. Perry, J.-E. Wahlund, A. Persoon, W. S. Kurth, J. Waite Jr., R. Perryman, M. Perry, J.-E. Wahlund, A. Persoon, and W. S. Kurth, "The ion composition of Saturn's equatorial ionosphere as observed by Cassini," *Geophysical Research Letters*, no. Cassini's Grand Finale, pp. 1–17, 2018.
72. M. W. Morooka, J.-E. Wahlund, L. Z. Hadid, A. I. Eriksson, N. J. T. Edberg, E. Vigren, D. J. Andrews, A. M. Persoon, W. S. Kurth, D. A. Gurnett, W. M. Farrell, J. H. Waite, R. S. Perryman, and M. Perry, "Saturn's Dusty Ionosphere," *Journal of Geophysical Research A: Space Physics*, vol. 124, pp. 1679–1697, 2019.
73. K. E. Miller, J. H. Waite Jr, R. S. Perryman, M. E. Perry, A. Bouquet, B. A. Magee, B. Bolton, T. Brockwell, M. M. Hedman, C. R. Glein, and J. Hopkins, "Cassini INMS constraints on the composition and latitudinal fractionation of Saturn ring rain material," *Icarus*, vol. 339, no. December 2019, p. 113595, 2020.